Accepted Manuscript

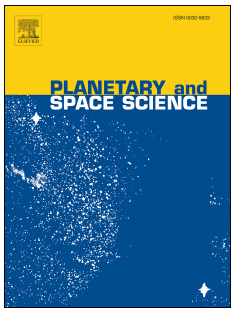

Electron-impact vibrational excitation of the hydroxyl radical in the nighttime upper atmosphere

L. Campbell, M.J. Brunger

PII: S0032-0633(17)30263-5

DOI: 10.1016/j.pss.2017.10.010

Reference: PSS 4412

To appear in: *Planetary and Space Science*

Received Date: 24 July 2017

Revised Date: 3 October 2017

Accepted Date: 16 October 2017

Please cite this article as: Campbell, L., Brunger, M.J., Electron-impact vibrational excitation of the hydroxyl radical in the nighttime upper atmosphere, *Planetary and Space Science* (2017), doi: 10.1016/j.pss.2017.10.010.

Electron-impact vibrational excitation of the hydroxyl radical in the nighttime upper atmosphere

L. Campbell[a], M. J. Brunger[a]

[a] *College of Science and Engineering, Flinders University, GPO Box 2100, Adelaide SA 5001, Australia*

Abstract

Chemical processes produce vibrationally excited hydroxyl (OH) in a layer centred at an altitude of about 87 km in the Earth's atmosphere. Observations of this layer are used to deduce temperatures in the mesosphere and to observe the passage of atmospheric gravity waves. Due to the low densities and energies at night of electrons at the relevant altitude, it is not expected that electron-impact excitation of OH would be significant. However, there are unexplained characteristics of OH densities and radiative emissions that might be explained by electron impact. These are measurements of higher than expected densities of OH above 90 km and of emissions at higher energies that cannot be explained by the chemical production processes. This study simulates the role of electron impact in these processes, using theoretical cross sections for electron-impact excitation of OH. The simulations show that electron impact, even in a substantial aurora, cannot fully explain these phenomena. However, in the process of this investigation, apparent inconsistencies in the theoretical cross sections and reaction rates were found, indicating that measurements of electron-impact excitation of OH are needed to resolve these problems and scale the theoretical predictions to allow more accurate simulations.

Keywords: hydroxyl radical, electron impact, vibrational excitation, mesosphere

*Corresponding author. Email: laurence.campbell@flinders.edu.au

1. Introduction

Several infrared emission lines from the night sky, between 725.14 and 896.22 nm, were identified by Meinel (1950a) as being due to the rotation-vibration spectrum of OH. Soon thereafter, Meinel (1950b) deduced that a chemical mechanism was likely the source of the excited OH. Simulations of observations supported that mechanism, while assumed auroral sources were shown to be due to contamination. The emissions from the excited OH were used to measure temperatures in the mesosphere and substantial effort was made to show that these were not affected by auroral input. Nevertheless, there are several characteristics of the observations which are not explained by the theory, such as higher OH densities at greater heights and weak emissions at energies higher than the maximum set by the chemical mechanism. Thus this work aims, using simulations, to investigate whether electron impact, by both thermal and auroral electrons, has any input to the OH emissions.

Measurements of cross sections for electron impact excitation of OH are not yet available, so simulations in this work are based on a theoretical approach by Riahi et al. (2006). Difficulties were encountered in reproducing the results of Riahi et al. using their formulae, in that the calculated rates for excitation of the OH[$A^2\Sigma^+$] state in the current implementation were smaller by a factor of 8. However, the current implementation was able to reproduce the results of Teulet et al. (1999) for O_2, who used the same formulation as Riahi et al. Thus there is a need for experimental measurements to resolve this discrepancy.

The method of Riahi et al. (2006) does not take account of branching between various final vibrational levels, although in principle this might be achieved by a normalisation to experimental data if that were available for OH. Hence this work introduces a method to determine a distribution between excitation to various vibrational levels.

The calculated cross sections were applied to determine excited populations and emission rates due to the impact of thermal or auroral electrons in the upper atmosphere. These were in all cases much smaller than the populations and rates due to the chemical reaction and hence do not explain the discreapancies between the chemical theory and observations. However, the investigation has flagged problems in the existing theoretical method for calculations of electron-impact excitation of OH and casts doubt on theoretical rates that have been used in simulations of plasma processes (Bruggeman

et al., 2010).

In Sec. 2 the theory of the production of the OH layer in the mesosphere is outlined, with discrepancies between simulations and observations identified. The method to calculate cross sections and excitation rates for electron-impact excitation of OH is also described here. In Sec. 3 the current implementation of the theory of Riahi et al. (2006) is discussed and verified and an extension of the theory to excitation of vibrational levels of the ground state is described. The atmospheric computation model is also described. These are then applied in simulations presented in Sec. 4 to show the relative populations and emissions due to electron impact and the chemical processes, leading to the conclusions in Sec. 5.

2. Background

2.1. OH layer measurements and theory

Meinel (1950b) observed that the intensities of OH emissions from the upper atmosphere were larger for higher vibrational levels, with no emissions for vibrational levels above $\nu = 9$. Meinel suggested that it is very likely that the observed bands are due to an energy resonance selectively populating level 9. Bates and Nicolet (1950) argued that this was most likely due to the reaction

$$\mathrm{H} + \mathrm{O_3} \rightarrow \mathrm{OH}' + \mathrm{O_2} \tag{1}$$

as the available 76 kcals (3.814 eV) of excess energy would explain the absence of excitation above level 9. However, Anlauf et al. (1968) showed in laboratory measurements that chemiluminescence from levels 8 and 9 of the ground electronic state of OH was substantial. Charters et al. (1971) updated this to relative populations of < 0.4, ≈ 0.4, ≈ 0.8 and 1.00 for ν =6, 7, 8 and 9.

Nicolet (1970) considered the reaction

$$\mathrm{O} + \mathrm{HO_2} \rightarrow \mathrm{O_2} + \mathrm{OH}^*_{\nu \leq 6} + 55 \text{ kcal}/2.4\text{eV} \tag{2}$$

noting that it could only play a role in the upper mesosphere. Takahashi and Batista (1981) subsequently found experimental evidence for this reaction occurring. Since then it has been contentious (Xu et al., 2012) with some researchers including it (e.g. (Grygalashvyly, 2015)) while others (Adler-Golden, 1997) did not. A simultaneous measurement of levels 1–9, including what is claimed to be the first measurement of the $\nu = 1$ population, was

reported by Migliorini et al. (2015). These are claimed to agree with the model of Xu et al. (2012), based on Eq. (1)

Harang and Pettersen (1967) compared nightglow and auroral spectra, looking carefully at the 6-1 band of OH to see if it contaminated the H_α line. There was no obvious enhancement of this band by the aurora. Harrison (1970) looked for but found no significant correlation between auroral and hydroxyl emissions (1.02–1.03 μm). Romick (1973) found an OH enhancement in the 937.0-nm region was probably due to contamination by NI lines and declared all previously reported aurorally associated enhancements to be suspect.

When observing mesospheric temperatures in auroral conditions a major concern is contamination of the OH bands by emissions from other species. Sigernes et al. (2003) stated that "No auroral effects have so far been reported/observed to influence the OH temperature series." Phillips et al. (2004) examined this in detail for the OH(8-3) band while Greet et al. (1998) did so for the OH(6-2) band. French (2002) examined the contamination of OH lines by auroral lines and also unthermalised OH lines. French and Klekociuk (2011) measured rotational temperatures from the P-branch lines of the OH(6-2) band to determine the variation over a 16-year interval. They found no dependence of the derived temperature on auroral activity (indicated by the atomic oxygen line at 844.6 nm). Nevertheless this does not rule out electron-impact vibrational excitation because temperature measurements depend on ratios of rotational lines, which reach thermal equilibrium much faster than vibrational levels. Hence the lack of correlation between OH-derived temperatures and aurora does not rule out an auroral contribution to vibrational excitation. Suzuki et al. (2010) reported observing an increase in the OH rotational temperature during an active aurora event, but only on one out of six suitable nights. They attributed the observations to auroral depletion of OH in the upper part of the OH layer.

Thus there is no definitive evidence for electron-impact effects on OH in the mesosphere. However, there are observations that are not explained by existing models:

- observations of emissions of much higher intensity than predicted at greater heights (McDade et al., 1987) and
- observations of emission from OH($\nu = 10$) (Osterbrock and Fulbright, 1998).

Hence it is *a priori* interesting to investigate the role of electron impact on OH in the mesosphere. To do this cross sections for electron-impact vibrational excitation are required, but no measurements are available. Theoretical calculations by Chen and Morgan (1997) are available for electron impact excitation of only the first vibrational level. These are not sufficient for this work, where there is a need to calculate excitation to levels $\nu = 8$ and 10, including from $\nu = 7$ and 9. The only option identified is to take the theoretical formulation of Riahi et al. (2006), which was used to calculate rates for excitation to electronic excited states of OH, and adapt it to excitation of vibrational levels in the ground state.

2.2. Electron impact cross sections for excitation of hydroxyl

Riahi et al. (2006) present formulae to calculate cross sections for electron-impact excitation of OH, as a starting point for calculation of excitation rates as a function of temperature. However it is necessary to refer to the work of Teulet et al. (1999) for many details, including an "elementary cross section" (originally put forward by Drawin (1968) and developed further by Bacri and Medani (1980)).

Riahi et al. (2006) specify the excitation cross section $Q_{T_1}^{T_2}$ for incident electron energy ε as:

$$Q_{T_1}^{T_2}(\varepsilon, \theta_e, \theta_g) = \frac{1}{Z(T_1, \theta_e, \theta_g)} \sum_{\nu_1=0}^{\nu_L(T_1)} \exp\left(-\frac{G(\nu_1)}{k\theta_e}\right) \times \sum_{J_1=0}^{J_L(\nu_1)} (2J_1 + 1) \exp\left(-\frac{F_{\nu_1}(J_1)}{k\theta_g}\right) \times \sum_{\nu_2=0}^{\nu_L(T_2)} \sum_{J_2=0}^{J_L(\nu_2)} \delta(J_2, J_1 \pm 2) \int_0^\infty P_{\nu_1}(r) q_{T_1,\nu_1 J_1}^{T_2,\nu_2,J_2}(r, \varepsilon) dr \quad (3)$$

where T is the electronic state, ν the vibrational level and J the rotational number, each with subscripts 1 and 2 indicating the initial and final case. θ_e and θ_g are the background electron and gas temperatures and k is Boltzmann's constant. Z is the two-temperature internal partition function of electronic state T_1, given by Teulet et al. (1999) as $Z(T_1, \theta_e, \theta_g) = \theta_g/\theta_e Z(T_1, \theta =$

$\theta_e = \theta_g$) where:

$$Z(T_1, \theta = \theta_e = \theta_g) = \sum_{\nu_1=0}^{\nu_L(T_1)} \exp\left(-\frac{G(\nu_1)}{k\theta}\right) \sum_{J_1=0}^{J_L(\nu_1)} (2J_1+1) \exp\left(-\frac{F_{\nu_1}(J_1)}{k\theta}\right). \tag{4}$$

$\nu_L(T_1)$ is the maximum vibrational quantum number for state T_1 and $J_L(\nu)$ is the maximum rotational quantum number for vibrational level ν. G and F are the vibrational and rotational energies given by:

$$G(\nu_1) = \left(\nu_1 + \frac{1}{2}\right)\omega_e - \left(\nu_1 + \frac{1}{2}\right)^2 \omega_e x_e + \left(\nu_1 + \frac{1}{2}\right)^3 \omega_e y_e \tag{5}$$

and

$$F_{\nu_1}(J_1) = B_{\nu_1} J_1(J_1+1) - D_{\nu_1} J_1^2 (J_1+1)^2, \tag{6}$$

where $B_{\nu_1} = B_e - \alpha_e(\nu_1 + \frac{1}{2})$ and $D_{\nu_1} = \beta_e(\nu_1 + \frac{1}{2})$. The probablility P is given by Riahi et al. (2006) as:

$$P_{\nu_1}(r) = \frac{1}{2^{\nu_1}\nu_1!}\sqrt{\frac{\alpha}{\pi}} \exp(-\alpha(r-r_e)^2) H_{\nu_1}^2(\chi), \tag{7}$$

where $\chi = \sqrt{\alpha}(r - r_e)$, $\alpha = (2\pi)/h)\sqrt{\mu k_0}$, $k_0 = 4\pi^2 c^2 \mu w_e^2$, c is the speed of light, h is Planck's constant, μ is the reduced mass of the molecule and r_e is the equilibrium internuclear distance. Riahi et al. (2006) define H_{ν_1} as the Hermitian (assumed here to be Hermite) polynomial of the ν_1^{th} degree. The elementary excitation cross section $q_{T_1,\nu_1,J_1}^{T_2,\nu_2,J_2}(r,\varepsilon)$ at internuclear radius r for an impacting electron of energy ε is given by Teulet et al. (1999) as:

$$q_{T_1,\nu_1,J_1}^{T_2,\nu_2,J_2}(r,\varepsilon) = 4\pi a_0^2 \alpha_{g_1 g_2} \xi \left(\frac{U_{12}-1}{U_{12}^2}\right), \tag{8}$$

where $U_{12} = \varepsilon/\Delta U$, $\Delta U = U(T_2,\nu_2,J_2,r) - U(T_1,\nu_1,J_1,r)$, a_0 is the Bohr radius, ξ is the number of optical electrons in state T_1 and $\alpha_{g_1 g_2}$ is a normalisation factor that depends on the spin multiplicities $g_i = 2S_i + 1$ of the initial and final states. U is the Morse potential function:

$$U(T_e,\nu,J,r) = T_e + G(\nu) + (D_e - G(\nu))[1 - \exp(-\beta_0(r-r_e))]^2 + \frac{h}{8\pi^2\mu c}\frac{J(J+1)}{r^2} \tag{9}$$

with

$$\beta_0 = 2.43534 \times 10^7 (\mu_A \omega_e x_e)^{0.5}, \tag{10}$$

where μ_A is the reduced mass in atomic units and D_e is the dissociation energy measured from the lowest value of the potential curve (Herzberg, 1989). The ionization cross section is:

$$q^{T_2,\nu_2,J_2}_{T_1,\nu_1,J_1}(r,\varepsilon) = 2.66\pi a_0^2 \left(\frac{E_1^{\rm H}}{\Delta U}\right) \alpha_{g_1 g_2} \xi \left(\frac{U_{12}-1}{U_{12}^2}\right) \ln(1.25 U_{12}), \tag{11}$$

where $E_1^{\rm H}$ is the ionization energy of the hydrogen atom.

The spectroscopic constants are given in Table 2 of Riahi et al. (2006), with values of $\alpha_{g_1 g_2}$ given in their Table 4. Riahi et al. specify two constraints in implementing the equations above: the range of r over which the integration is performed is limited to where $P_{\nu_1}(r) > 0.001$ of the maximum value, and also to the stability area (under the horizontal lines in our Fig. 1) where the molecule would not immediately dissociate.

3. Implementation: methods and verification

3.1. OH cross sections

Problems were encountered in reproducing results from Riahi et al. (2006), so initially the current implementation was tested by reproducing results given by Teulet et al. (1999). In Fig. 1 the calculated potential curves and stability areas for 4 excited levels of O_2 are compared with those plotted by Teulet et al. (1999) in their figure 2. There are substantial differences. These differences are largely eliminated by replacing Eq. 10 with equation (III,100) from Herzberg (1989):

$$\beta = 1.2177 \times 10^7 \omega_e \sqrt{\frac{\mu_A}{D_e}} \tag{12}$$

(assuming that β_0 is the same quantity as β of Herzberg (1989)). The remaining differences are removed by replacing D_e with the dissociation energy D_0 throughout the calculation, giving the dashed curves in Fig. 1 that are in good agreement with the values of Teulet et al. (1999).

These two formulations were then applied to produce the cross sections for the $O_2[X^3\Sigma_g^-] \rightarrow O_2^+[X^2\Pi_g]$ ionization in figure 4 of Teulet et al. (1999). In Fig. 2 the current implementation for the specified model of Teulet et al.

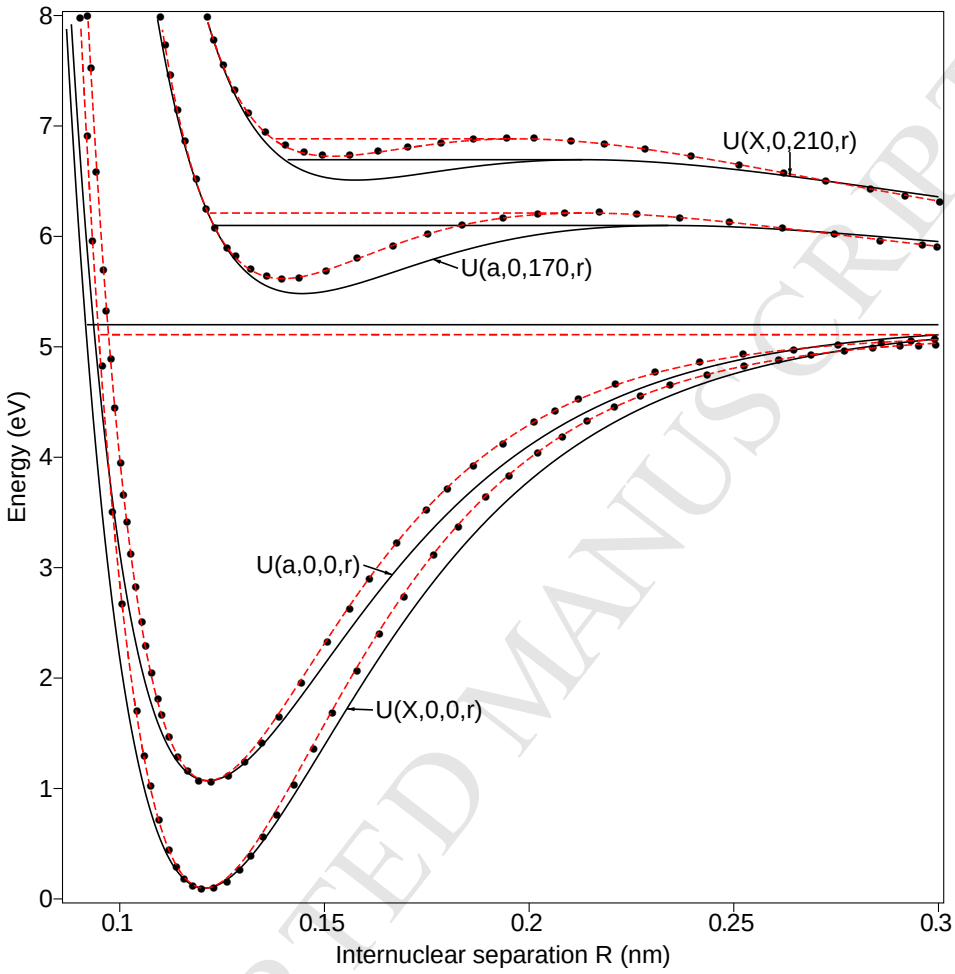

Figure 1: A comparison of computed potential curves with values (•) digitised from figure 2 of Teulet et al. (1999). Computed curves are given for the current implementation of the calculation specified by Teulet et al. (—) and of that calculation with the modifications described in the text (– – –). Horizontal lines show the "stability areas".

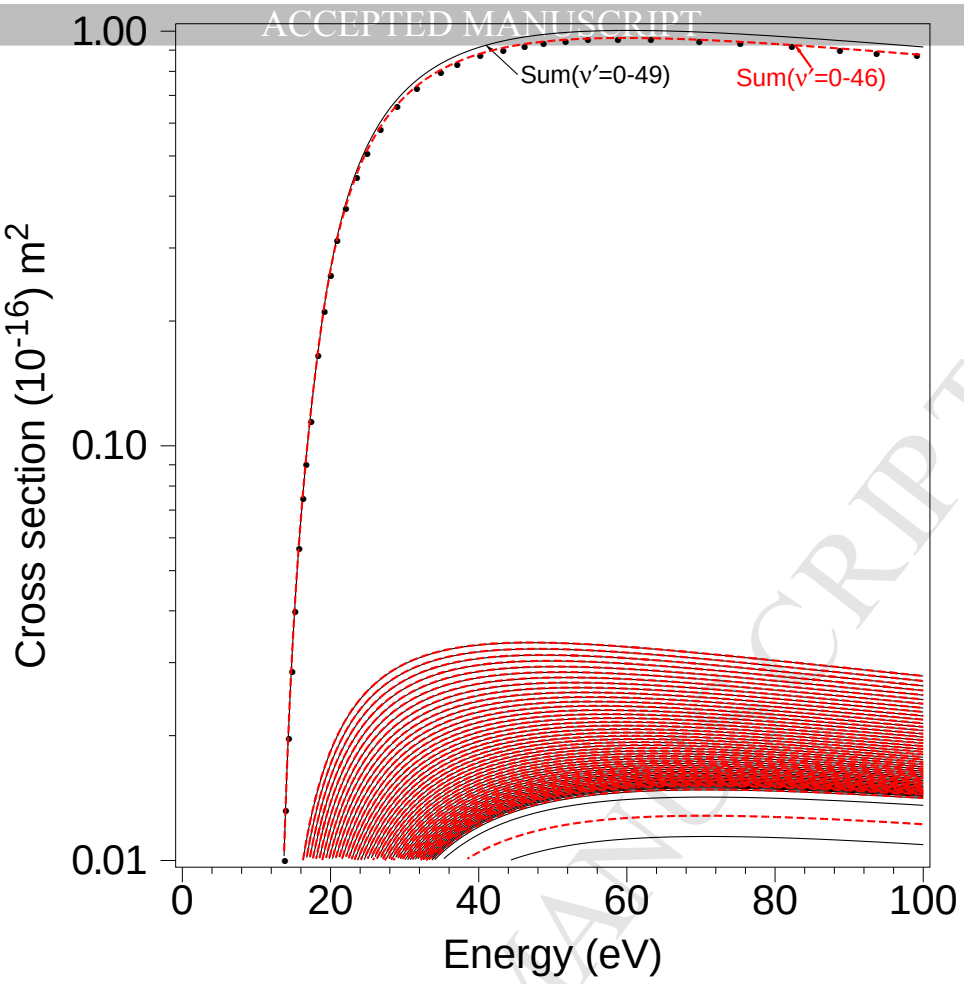

Figure 2: A comparison of the cross sections for electron impact ionisation $O_2[X^3\Sigma_g^-] \rightarrow O_2^+[X^2\Pi_g]$ with values digitised from Fig. 4 of Teulet et al. (1999) (•). The solid curves show the results of the implementation of the model of Teulet et al. The dashed curves result from addition of the modifications $D_e = D_0$ and using the Herzberg β_0. Both curves are labelled with the range of upper levels that contribute to the sum. The unlabelled curves are the cross sections for individual vibrational levels of the final state.

(1999) is shown by solid curves and for the modified case (using Eq. (12) and D_e replaced by D_0) by dashed lines. Again there is much better agreement between the current calculations and those of Teulet et al. (1999) for the modified case. The individual contributions for transitions to the various upper levels are shown for information.

Teulet et al. (1999) and Riahi et al. (2006) calculated excitation rate coefficients as functions of temperature for Maxwellian electron energy distributions using:

$$R_{T_1}^{T_2}(\theta_e, \theta_g) = 2\left(\frac{2}{\pi m_e}\right)^{0.5} (k\theta_e)^{-1.5} \int_0^\infty \varepsilon Q_{T_1}^{T_2}(\varepsilon, \theta_e, \theta_g) \exp\left(-\frac{\varepsilon}{k\theta_e}\right) d\varepsilon \quad (13)$$

where m_e is the electron mass.

The current implementation was run with various constraints, as shown in Fig. 3, to compare with the rate coefficients for the $O_2[X^3\Sigma_g^-] \rightarrow O_2[a^1\Delta_g]$ excitation presented in figure 5 of Teulet et al. (1999). These are 7 individual calculated values ($\circ$) digitised from their figure and their fit (—) to those values. In the upper panel the ratios of the current calculated values to those of Teulet et al. are plotted. Error bars show the digitisation error, estimated from discrepancies between the digitised temperatures and integer multiples of 2000 K. The current calculation with only the probability constraint gives discrepancies of up to 25%. These are considerably reduced by adding the stability constraint. Including the modifications of $D_e = D_0$ and the Herzberg β_0 reduces the differences to the magnitude of the digitisation error. This shows that the current implementation is at worst very close to an accurate reproduction of the method of Teulet et al.

As Riahi et al. (2006) did not present any calculated OH excitation cross sections, the only option for comparison is with their calculated values of rate coefficients versus temperature. In Fig. 4 the current calculations for excitation rate coefficients of the $OH[A^2\Sigma^+]$ state are compared with values from their table 11 and their fitted formula. With both the probability and stability constraints applied the values in the current implementation are about 1/8 of their values. Excluding initial predissociative levels from Eqs. (3) and (4) improves the fit to the shape of their fitted curve. In this case the modifications that improved the agreement with the values of Teulet et al. (1999) each reduce the agreement with the shape, although the $D_e = D_0$ case produces agreement with the absolute values above 10000 K.

Thus the current implementation can reproduce the absolute values of excitation rate coefficients given by Teulet et al. (1999) for O_2, but can only reproduce the coefficients for $OH[A^2\Sigma^+]$ of Riahi et al. (2006) if these are reduced by a factor of 8. This discrepancy is of some concern due to the use of the rate coefficients of Riahi et al. in plasma modelling (Bruggeman et al., 2010) and so ultimately needs to be resolved by measurements of the relevant cross sections.

3.2. Ground-state vibrational cross sections

The only cross sections for ground state vibrational excitation of OH found in the literature were those of Chen and Morgan (1997), who used the R-matrix method to calculate the total integrated cross section for low-energy electron impact excitation of the $\nu = 1$ vibrational level of OH, as

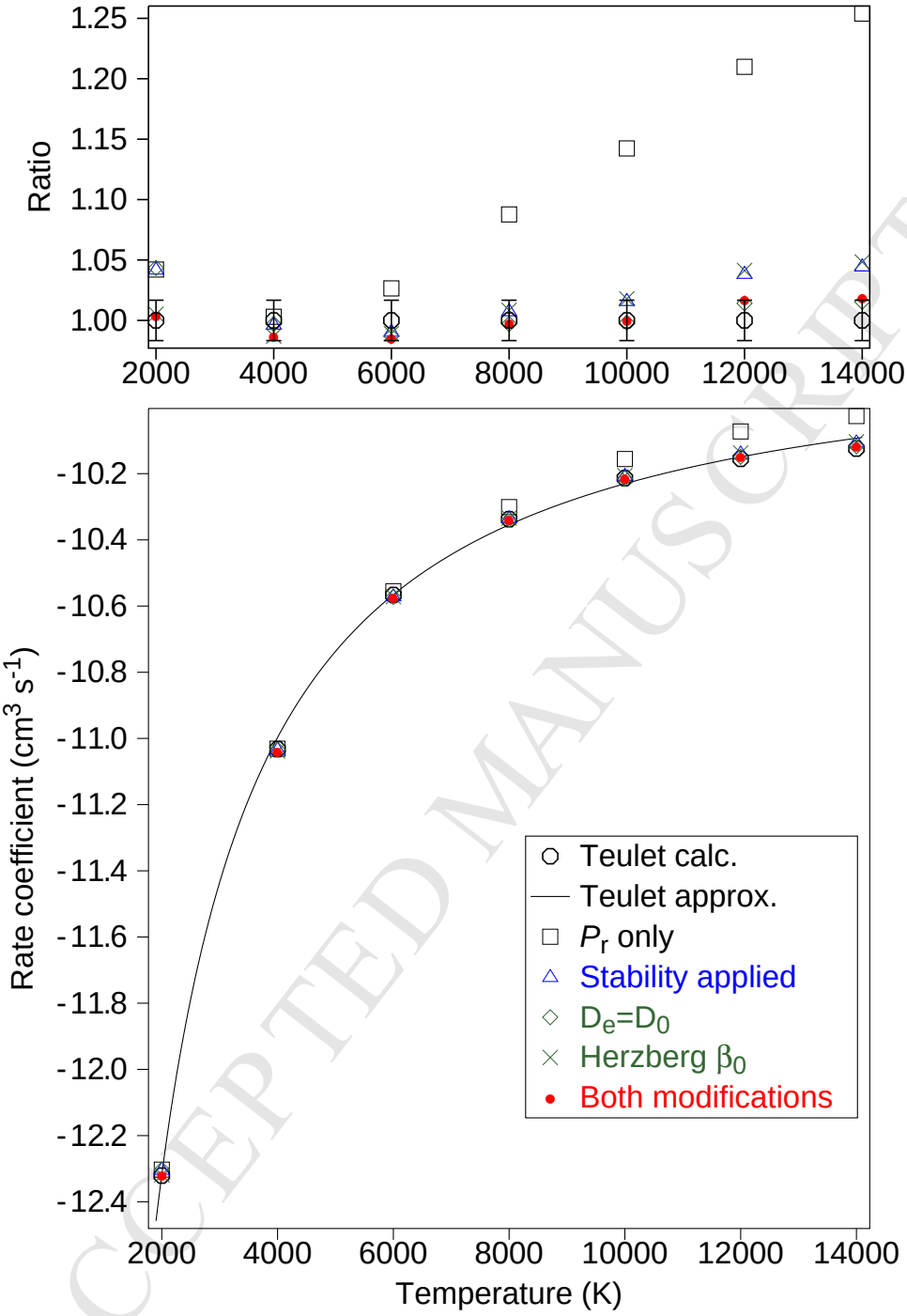

Figure 3: A comparison of rate coefficients for excitation of the $O_2[a^1\Delta_g]$ state given by the current calculation with the values of Teulet et al. (1999). The curve shows the approximate formula fitted by Teulet et al. to their calculated values (○). The current implementation of Teulet's formula is shown for the probability constraint only (□), then addition of the stability constraint (△), then addition of the modifications $D_e = D_0$ (◇) or the Herzberg β_0 (×), then finally with both these modifications (•). In the upper panel all values are replotted as a ratio to the calculated values (○) of Teulet et al. The error bars are an estimate of the digitisation error.

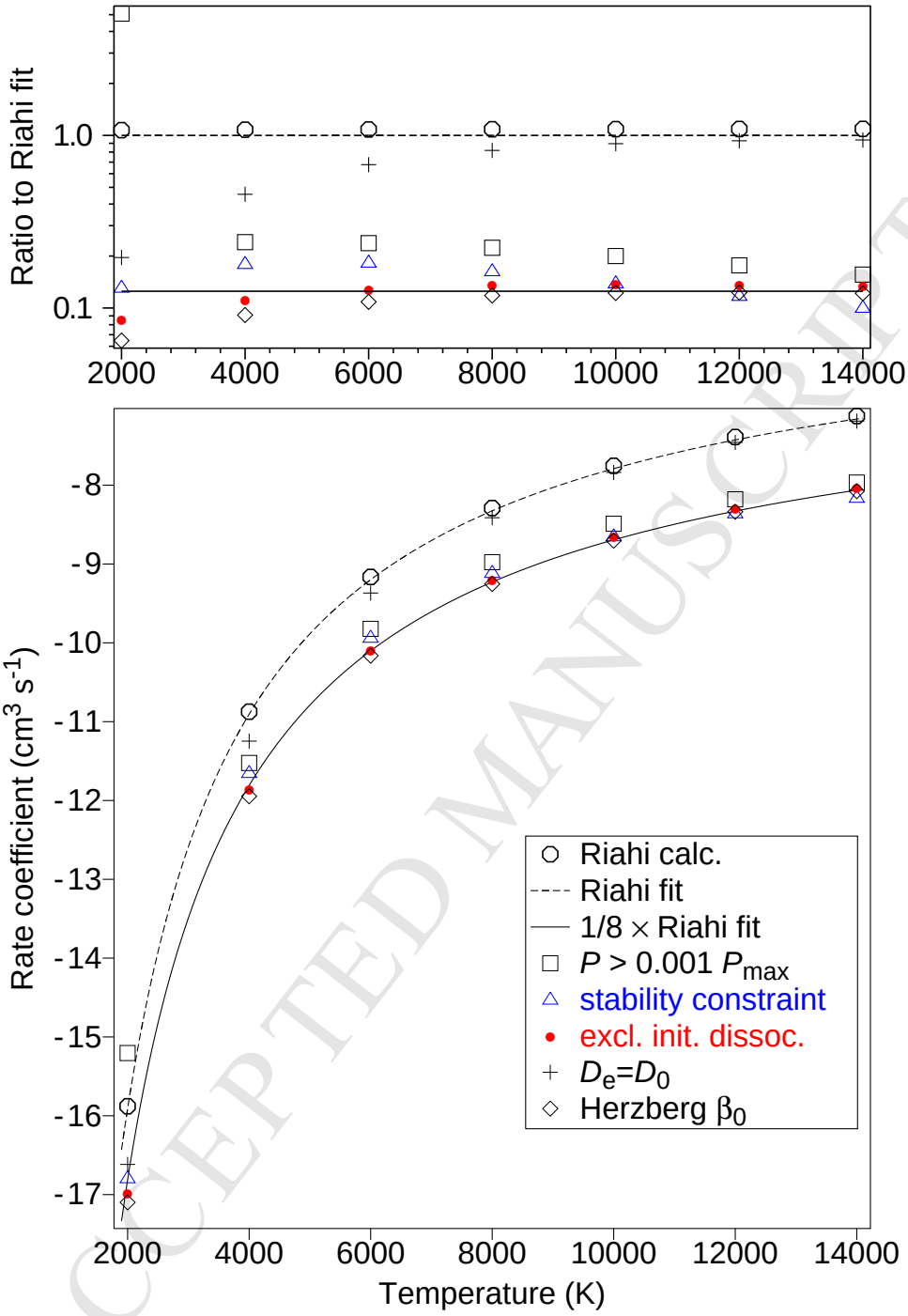

Figure 4: A comparison of rate coefficients for electron impact excitation of the OH[$A^2\Sigma^+$] state given by the current calculation with the values of Riahi et al. (2006). The dashed curve shows the approximate formula fitted by Riahi et al. to their calculated values. The current implementation of Riahi's formula is shown for the probability constraint only (□), then addition of the stability constraint (△), then elimination of predissociated initial levels (•), then application of the modifications $D_e = D_0$ (+) or the Herzberg β_0 (◇). A solid curve shows Riahi's fit divided by 8. In the upper panel all values are replotted as a ratio to the fitted curve of Riahi et al.

shown in Fig. 5. As this study requires cross sections for several other transitions (e.g. $0 \rightarrow 10$), the only option currently available was to apply the approach of Riahi et al. (2006), which includes all upper vibrational levels. However, Riahi et al. did not apply their method to electron-impact excitation to vibrational levels of the ground state of OH, so it is necessary here to investigate the application in detail, to ensure that the results are physically reasonable.

The required constants that were not available from Riahi et al. (2006), $\omega_e y_e$ and $\omega_e z_e$, were taken from table 3 in Brooke et al. (2016). The maximum values of J_L were determined as those that provide a stability area in the potential curve, rather than a monotonically decreasing potential with increasing r.

Application of Eq. (3) at 300 K produces the curve for the $0 \rightarrow 1$ excitation shown in Fig. 5. It is significantly different to the calculated results of Chen and Morgan (1997), particularly in the energy of the maximum cross section, the absence of resonances and the absence of a drop at 0.85 eV due to the opening of the $\nu = 2$ channel. The latter suggests that a term is missing in Eq. 3 to allow for the branching between upper vibrational levels. The curve for the $0 \rightarrow 2$ cross sections has the same maximum value as for $0 \rightarrow 1$, which is further evidence that branching between different upper levels is not accounted for in the formulation of Riahi et al. For example, measurements by Noble et al. (1996) for electron-impact excitation of vibrational levels $\nu = 1 - 4$ in the ground state of O_2 show a decrease in maximum cross section with increasing ν. Note that as resonances are ubiquitous in electron–molecule scattering (Brunger and Buckman (2002) and Brunger (2017)), their absence in the formulation of Riahi and colleagues strongly suggests a limitation in that approach.

The cross sections calculated for the $0 \rightarrow 0$ (i.e. excitation or deexcitation to other rotational levels of the $\nu = 0$ vibrational level) excitation are also plotted in Fig. 5. Deexcitation is implemented using (Makabe and Petrovic, 2014):

$$Q_s(\varepsilon) = \frac{g_0}{g_j} \frac{\varepsilon + \varepsilon_j}{\varepsilon} Q_j(\varepsilon + \varepsilon_j), \tag{14}$$

where Q_s is the cross section for a superelastic collision from state j (with a threshold energy of excitation ε_j and statistical weight g_j) produced by an electron of energy ε. As all the rotational levels are of different energies all statistical weights are unity in this work.

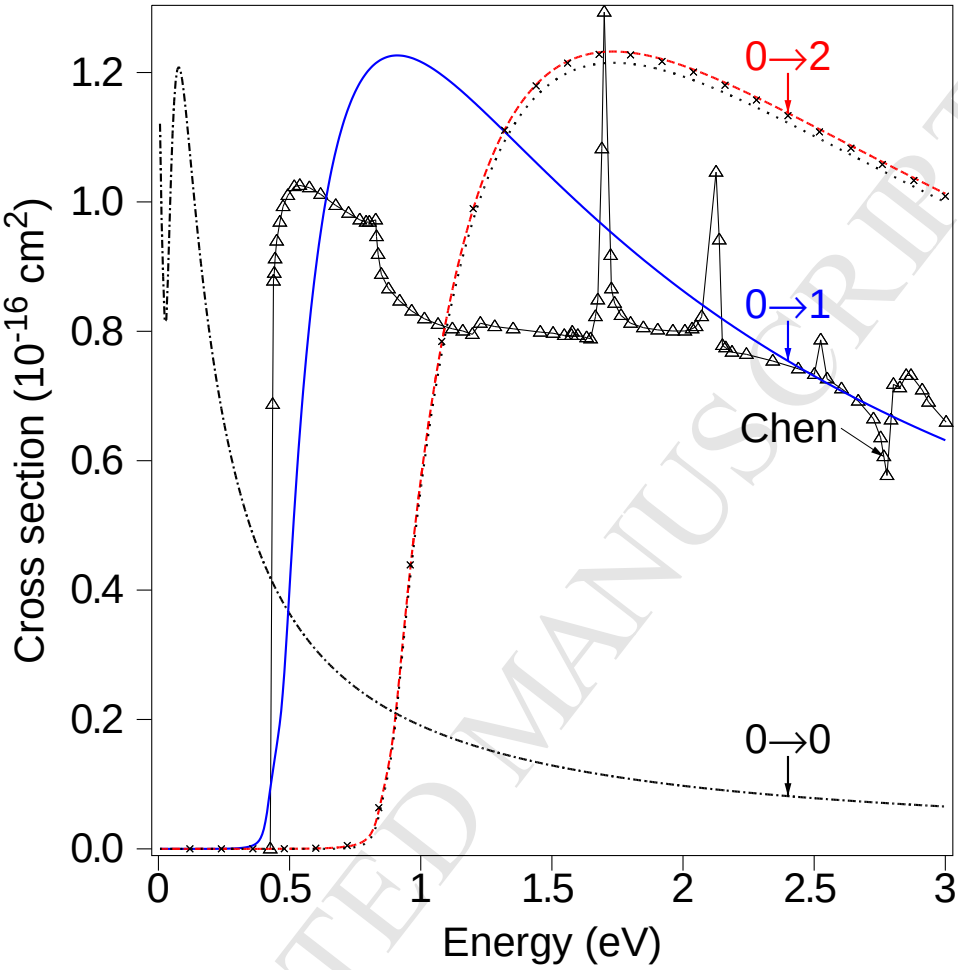

Figure 5: Theoretical cross sections for electron-impact excitation of vibrational levels of the ground state of OH at 300 K: digitised values of Chen and Morgan (1997) (△—△) and the current calculation using Eq. (3) for $0 \rightarrow 0$ (- · - · -), $0 \rightarrow 1$ (—) and $0 \rightarrow 2$ (– – –). $0 \rightarrow 2$ cross sections are also shown for substitution of the spectroscopic constants of Brooke et al. (2016) (×) and for limiting the calculation to the region $P_0(r) > 0.05\times$ maximum probability (· · ·).

To investigate the significance of uncertainties in the calculations, $0 \rightarrow 2$ cross sections are plotted for calculations using the spectroscopic constants of Brooke et al. (2016) ($\times$) and for limiting the calculation to the region where $P_0(r) > 0.05\times$ maximum probability. The change due to the former is negligible, while the small change produced by the altered probability constraint indicates that the inaccuracy of the Morse potential at small r does not introduce a significant error.

Application of the same equation for $\nu_2 > 2$ produces cross sections with the same maximum value, leading to an increasing and unphysically large total excitation cross section with increasing impact energy. The missing term could be handled within the paradigm of Riahi et al. (2006) by setting a value of $\alpha_{g_1 g_2}$ for each vibrational level, based on experimental values. In the absense of these, an algorithm is applied here in which the cross sections given by Eq. (3) are scaled so that their sum is equal to the maximum cross section calculated for any individual contributing excitation, with the result shown by dashed curves in Fig. 6. Comparing the result for $\nu = 1$ with the calculation of Chen and Morgan (1997) shows a similar maximum value but a larger drop at the energy of the onset of the $\nu = 2$ excitation. This suggests that the cross sections of Chen and Morgan (1997) for $\nu = 2$ are smaller than given by the current algorithm. As the theory of Chen and Morgan is more rigorous than that of Riahi et al. it might be expected that it might be better. However, this can only be resolved either by measurements (as are being set up at Flinders University (Campbell and Brunger, 2016)) or the application of a more advanced theory for electron scattering from molecules, as has recently been applied to hydrogen by Zammit et al. (2017).

The dip in the $0 \rightarrow 0$ transition at about 0.47 eV seemed unphysical, suggesting that the branching algorithm is not correct, at least where the cross sections are close to being equal for two upper vibrational levels. As this might be explained by the varying weightings within the assemblages of rotational levels with changing impact energy, the calculation was performed with the branching between channels applied for each individual initial rotational level. This produced the cross sections shown by the solid curves in Fig. 6. The difference in the cross sections is only apparent near crossover points and appears negligible relative to the integrated cross section over all energies. Nevertheless, due to the large decrease in electron flux with increasing energy (Campbell et al., 2006) and the consequent large weighting of the contribution of cross sections at low energy, the difference may be significant, so in the subsequent modelling the distribution between upper

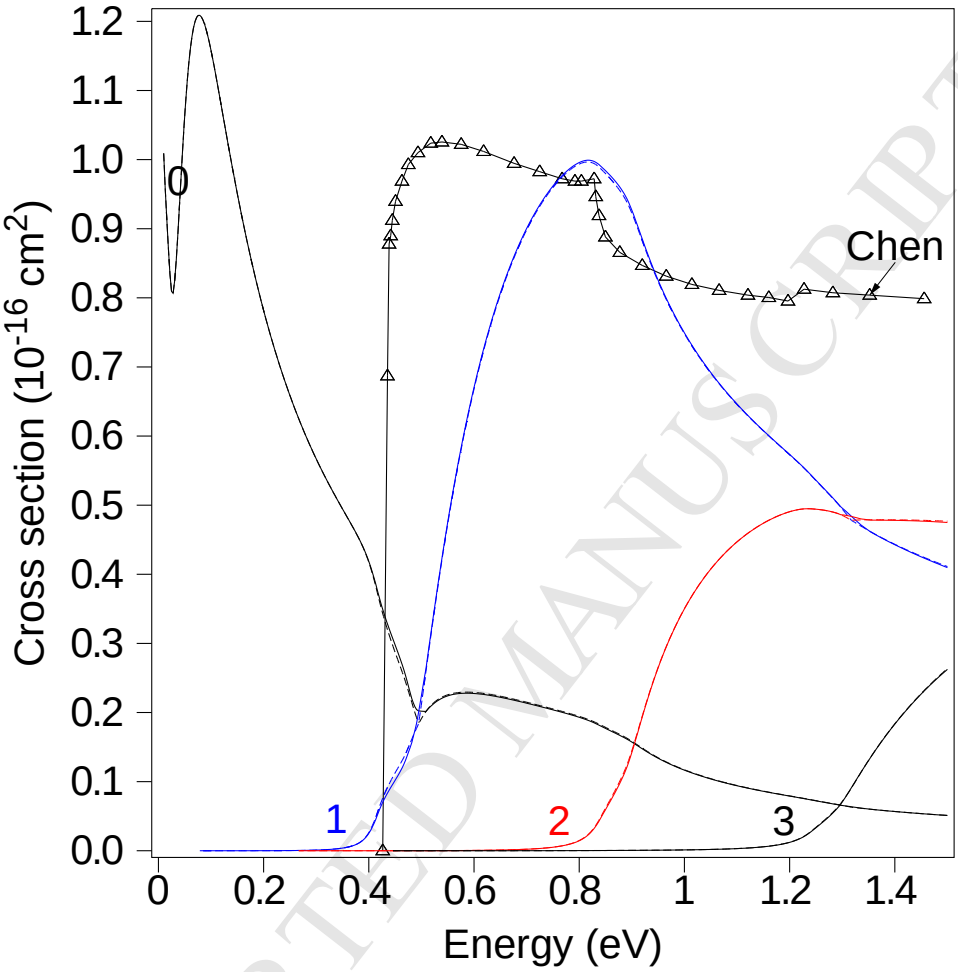

Figure 6: Theoretical cross sections for the $0 \rightarrow \nu$ transitions in the ground state of OH (curves as labelled for $\nu = 0, 1, 2, 3$), for the approximate allocation to different transitions (dashed curves) and for the detailed allocation for every initial rotational level (solid curves).

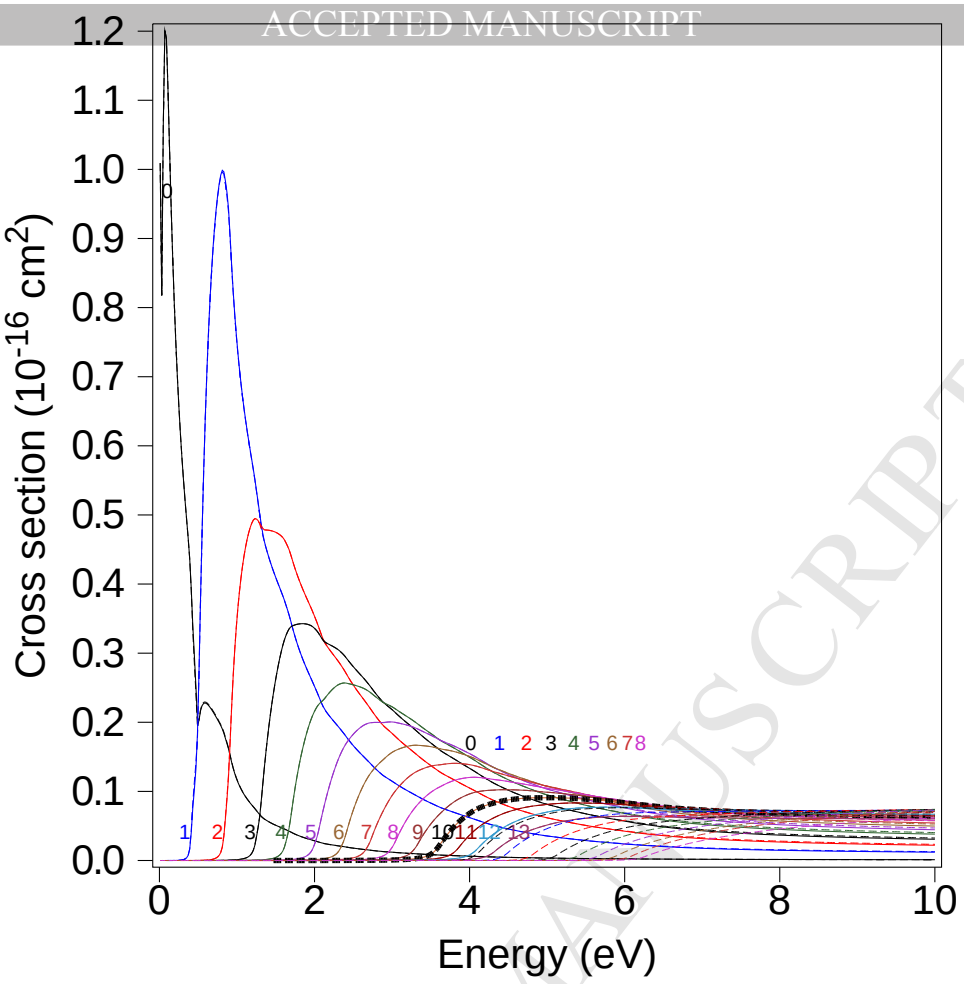

Figure 7: Theoretical cross sections for the 0→ ν transitions in the ground (—) and $A^2\Sigma^+$ (- - -) electronic states of OH (curves as labelled with ν). The 0 → 10 excitation in the ground state is highlighted (thick dashed line).

levels is calculated for each initial rotational level.

The full set of cross sections necessary for determination of the 0 → 10 excitation is shown in Fig. 7. Electrons with energies in the range for this excitation can also excite the $A^2\Sigma^+$ electronic state, so these are included in scaling down the cross sections for individual vibrational levels. (N.B. These cross sections are thus about one tenth of the values predicted by Eq. (3), implying that the coefficients of Riahi et al. in Fig. 4 are too large by a factor of 10, in addition to the factor of 8 found in the current emulation of their formula.)

The same procedure is used to calculate cross sections for excitation from vibrationally excited levels, such as the 9 → 10 transition with the term $\exp(-G(9)/k\theta_e)$ in Eqs. (3) and (4) set to 1. The resulting cross sections are shown in Fig. 8 for excitation and dexcitation from OH($\nu = 9$) to levels 0–13. Here the differences between applying the distribution between levels at the summed or individual rotational level are more apparent.

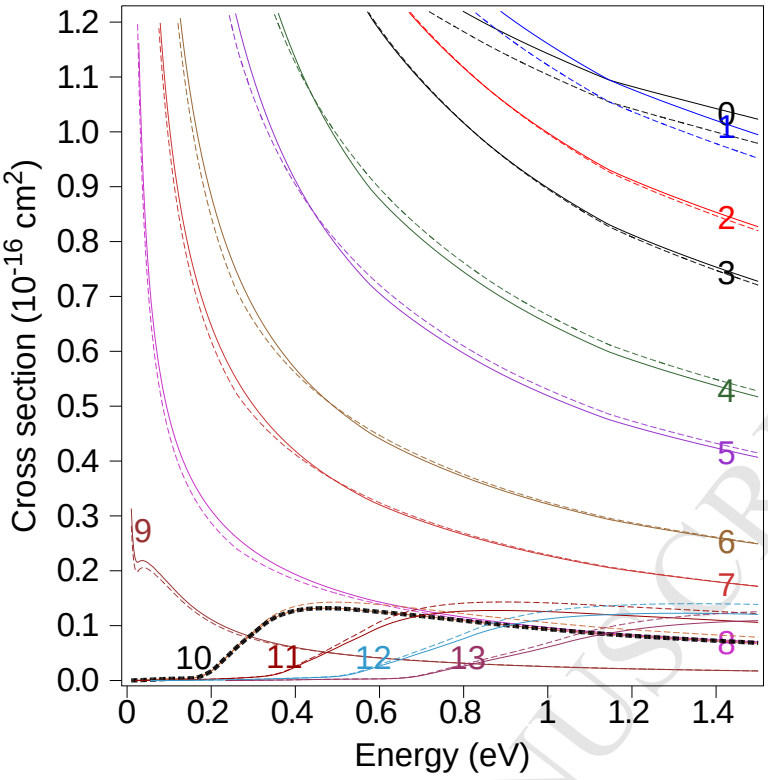

Figure 8: Theoretical electron-impact cross sections for $9 \rightarrow \nu$ transitions in the ground state of OH (curves as labelled with ν), with the distribution between levels determined by normalisation of cross sections for vibrational levels (dashed curves) and normalisation of transitions for each individual initial rotational level (solid curves).

3.3. Atmospheric modelling

The different atmospheric models used in this study were specified in text files, which were then converted to efficient computer code by a general computer program that was used for all models. This allowed easy implementation of the different models and variations without any possibility of making new coding errors when changing models.

A model was specified as a set of reactions, each with a reaction rate. These were then evaluated in an implicit time-step calculation, where a species with population density P_0, gain rate $G(t_0)$ and loss probability $L(t_0)$ at time t_0 has a population density of P_1 given by

$$P_1 = \frac{P_0 + G(t_0)\Delta t}{1 + L(t_0)\Delta t} \tag{15}$$

after a time interval Δt. An adaptive time step, in which Δt is calculated at each step so that the density of any species does not change by more than a specified fraction in that time step, was used. While the interactions involving excited OH (radiative transitions and quenching by N_2, O_2 and O)

are relatively fast, so that an equilibrium calculation could be performed, the density of O_3 takes much longer to reach equilibrium, so the time-step calculation was necessary to confirm that the O_3 and OH densities reached close to equilibrium within the necessary time (of about 3 hours).

Electron impact was included in this method by calculating electron-impact excitation rates and inserting them as reaction rates. For thermal electrons Eq. (13) was used, with θ_g determined from the MSISE-90 atmospheric model (Hedin, 1991)) and electron density and θ_e from the IRI-2007 model (Bilitza and Reinisch, 2008). Auroral electron fluxes were calculated as described by Campbell et al. (2006), with the exception of the auroral flux below 130 km, where that of Campbell et al. at 130 km was scaled down in proportion to the electron energy flux measurements of McEwen and Venkatarangan (1978). The secondary electrons produced by auroral impact produce a thermal electron population with higher densities and temperatures. This enhanced thermal population was modelled using an electron density profile measured in auroral conditions (Miyoshi et al., 2015) and an electron temperature profile calculated by Rees and Walker (Vallance Jones, 1974). The non-Maxwellian auroral flux cannot be used in Eq. (13), but the rate coefficient is determined in a similar way by multiplying the flux by the cross sections at each energy and summing over all energies (Campbell and Brunger, 2013).

4. Simulations

As a basis for comparison and verification, this study emulated two cases in the literature where OH densities or emissions were calculated and compared with measurements. The input to these from electron-impact was then added, to investigate whether electron-impact makes a difference to vibrational excitation of OH.

Adler-Golden (1997) described a model (incorporating new transition probabilities by adjustment of values from Turnbull and Lowe (1989) and the MSISE-90 atmospheric model (Hedin, 1991)) to calculate parameters measured by Takahashi and Batista (1981) and several others. Their very good absolute agreement (within 30%) provided credibility for the model, which was also used to calculate number densities for the $\nu = 1, 3, 5, 7$ and 9 vibrational levels of OH as a function of height for the circumstances of the measurements by Takahashi and Batista (1981).

The current emulation of the calculation of Adler-Golden is shown in Fig. 9. Symbols showing the calculated values of the densities of vibrationally excited OH (for $\nu = 1, 3, 5, 7, 9$) show good agreement with the values (curves) digitised from figure 6 of Adler-Golden.

Eq. (13) was used to determine the part of the OH(1) population produced by electron excitation (+) in Fig. 9. The same populations ($\triangle$) were then determined by using the electron-flux calculation. The agreement of the two methods verifies the implementation of the electron-flux approach that is used below for auroral electrons.

A postulated profile for the density of OH($\nu = 10$), based on the observation by Osterbrock and Fulbright (1998) of a ratio of 1.6×10^{-3} for the OH($\nu = 10$) density to that of OH($\nu = 9$), is shown by circles. As the observations of Osterbrock and Fulbright were made at a low-latitude site, auroral input is not relevant and so only thermal electrons were considered. As the electron temperature is too low to produce the $0 \rightarrow 10$ excitation in OH, only the $9 \rightarrow 10$ excitation was included. In the absence of published values, the loss rates for OH($\nu = 10$) (radiative transitions and quenching) were assumed to be the same as the Adler-Golden values for OH($\nu = 9$). The resulting calculated populations produced by electron impact ($\bullet$) are very much less than the values based on ratio given by Osterbrock and Fulbright.

The above analysis was repeated for the place and time of rocket measurements to be considered below, which is at a higher latitude (57.4°N) appropriate for inclusion of auroral input. In this case the calculated populations for OH($\nu = 1, 3, 5, 7, 9$) are different to those of Adler-Golden for the low-latitude site, showing the sensitivity of the densities to location and time. Auroral excitation of OH($\nu = 10$) by both the $0 \rightarrow 10$ and $9 \rightarrow 10$ were added. Again the densities of OH($\nu = 10$) are very much less than the densities postulated to produce the emissions measured by Osterbrock and Fulbright (1998).

McDade et al. (1987) analysed a rocket flight P234H (Greer et al., 1986) that made simultaneous measurements of the OH(8-3) emissions and the atomic oxygen density. As many of the parameters (such as transition probabilities) were uncertain, they established ratios between parameters in order to remove the effect of uncertain values, allowing a calculation of the OH(8-3) emission that agreed well with the measurements. In Fig. 11 emulation of their model using the current computational program (—) agrees well with their measurements ($\times$) in the altitude range 81–95 km. Above 100 km the measured values are much higher than calculated. (N.B. McDade et al. did

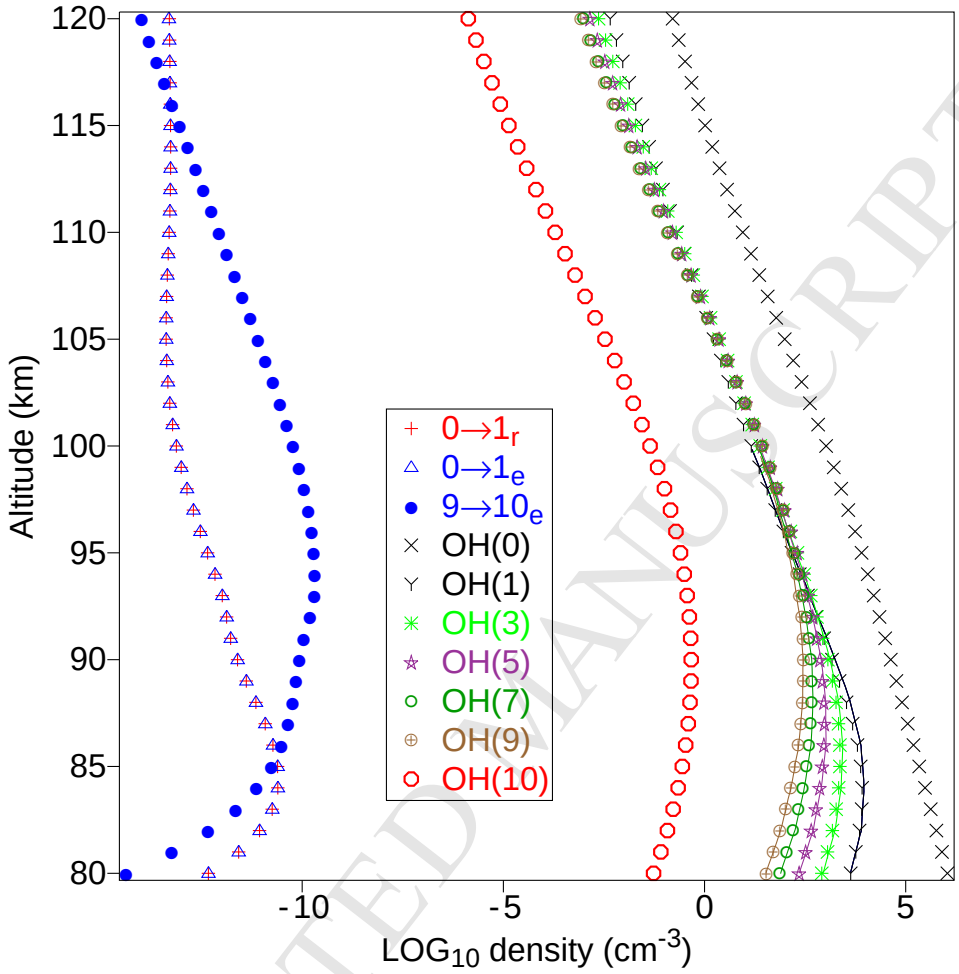

Figure 9: Emulation (symbols, as labelled) of the Adler-Golden model (—) of the densities of the $\nu = 1, 3, 5, 7, 9$ vibrational levels of OH. An approximation of the OH($\nu = 10$) level (large $\circ$) (based on the ratio of Osterbrock and Fulbright (1998)) and the population of this level ($\bullet$) due to impact of thermal electrons producing the OH($\nu = 9 \rightarrow 10$) transition are shown. The population of OH(1) due to electron impact is shown for calculations using Eq. 13 (+) and using the electron-flux method ($\triangle$).

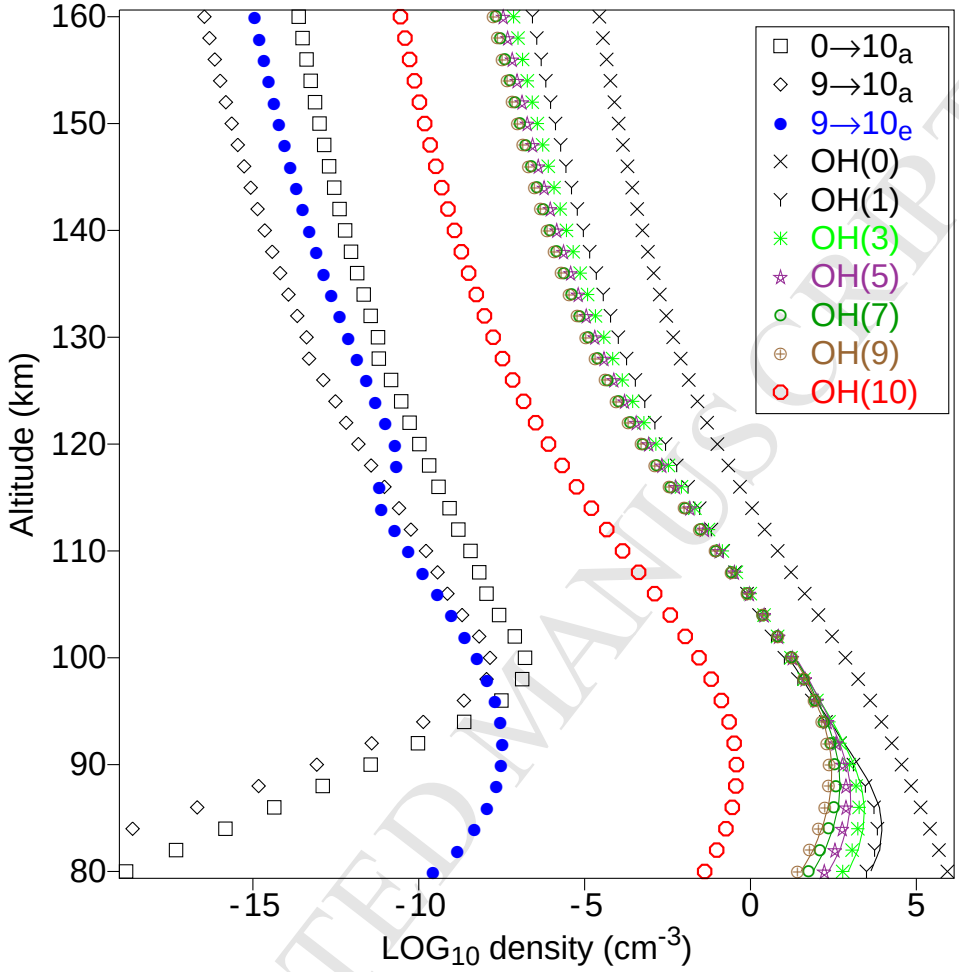

Figure 10: Current calculation of the densities of the $\nu = 1, 3, 5, 7, 9$ vibrational levels of OH and an approximation of the OH($\nu = 10$) level (large $\circ$) (based on the ratio of Osterbrock and Fulbright (1998)) at a higher latitude site. The populations of OH($\nu = 10$) due to electron impact are shown for thermal-electron ($\bullet$) and auroral-electron ($\Diamond$) impact producing the OH($\nu = 9 \rightarrow 10$) transition and auroral excitation of the OH($0 \rightarrow 10$) transition ($\Box$).

not make the comparison above 100 km.)

As the model of McDade et al. did not calculate populations of individual vibrational levels of OH, the model of Adler-Golden was used to include electron input. While this model does not agree well with the measurements below 93 km, it gives a similar result to the emulation of the McDade model above 100km, in that it predicts emissions much less than the measurements. Hence it is valid to use it to compare the electron-impact contribution to the population of OH($\nu = 8$) and so to the (8-3) emissions. These contributions are shown for auroral excitation of $0 \rightarrow 8$ and $7 \rightarrow 8$ transitions and (aurorally-enhanced) thermal-electron excitation of the $7 \rightarrow 8$ transition. In all cases the electron-induced emissions are far less than the chemically produced emissions and do not account for the deficit of the chemically-based models relative to the measurements above 100 km.

5. Conclusions

We have investigated the current knowledge of electron-impact excitation of OH, using a theoretical formulation that allows interactions between all vibrational levels to be calculated. Difficulties were encountered in reproducing some published results, so the discrepancies were investigated to confirm that the problem is not in the current implementation of the technique. This raises serious doubts about some published rates for excitation of OH($A^2\Sigma^+$) that have been used in plasma modelling (Bruggeman et al., 2010), as the current work finds that in the emulation of previous work the rate coefficients are a factor of 8 smaller, illustrating the need for measurements of the cross sections. To produce physically reasonable results it was necessary to adjust the theory of Riahi et al. (2006) to allow for branching between excitations to different vibrational levels (which produces a further $\sim$90% reduction in the cross sections for the $A^2\Sigma^+$ state). The cross sections calculated with this amended technique were applied to predict the contribution of electron impact to excitation of OH in the mesosphere, in addition to the principal chemical process. It was found that the contributions of both thermal- and auroral-electron impact to vibrational excitation are much smaller than those of the chemical processes and so do not account for differences between measurements and theoretical models for the production of the OH($\nu = 10$) vibrational level or the (8-3) emissions above 95 km. However, the calculated cross sections could be used to predict whether emissions from the OH($\nu = 10 - 13$) vibrational levels and the $A^2\Sigma^+$ state could be used as

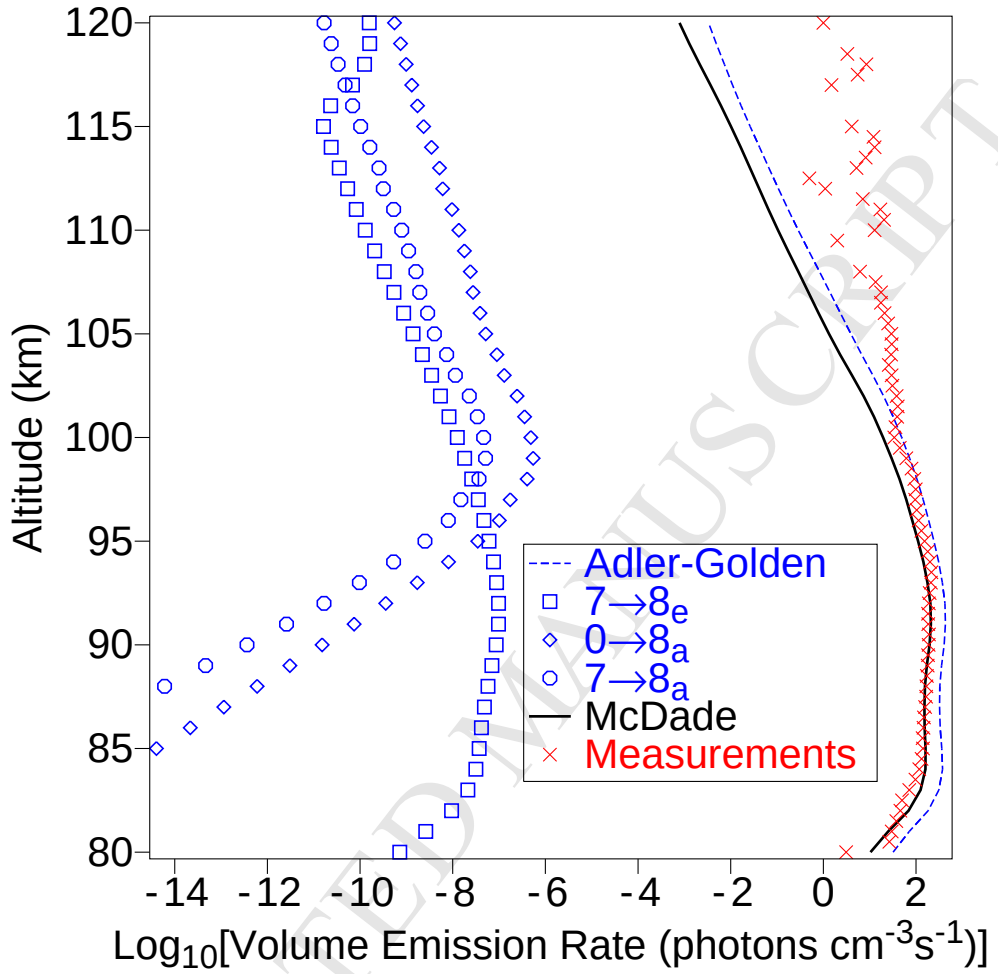

Figure 11: Measurements (×) of the (8-3) transition in the ground state of OH (McDade et al., 1987) compared with predictions: (—) the current emulation of Mcdade's fit; (- - -) the current emulation of the Adler-Golden model. The components of the (8-3) emissions due to thermal-electron excitation of the $7 \rightarrow 8$ transition (□), auroral-electron excitation of the $0 \rightarrow 8$ transition (◊) and auroral-electron excitation of the $7 \rightarrow 8$ transition (○) are shown.

tracers of secondary electrons produced in energetic particle events.

Acknowledgements

We thank the Australian Research Council for funding this work (grant number DP160102787).

References

Adler-Golden, S., 1997. Kinetic parameters for OH nightglow modeling consistent with recent laboratory measurements. J. Geophys. Res. 102, 19969–19976.

Anlauf, K. G., MacDonald, R. G., Polanyi, J. C., 1968. Infrared chemiluminescence from H + O_3 at low pressure. Chem. Phys. Lett. 1, 619–622.

Bacri, J., Medani, A., 1980. Electron diatomic molecule weighted total cross section calculation 1. Principles for calculation. Physica 101C, 399–409.

Bates, D. R., Nicolet, M., 1950. The photochemistry of atmospheric water vapor. J. Geophys. Res. 55, 301–327.

Bilitza, D., Reinisch, B. W., 2008. International Reference Ionosphere 2007: Improvements and new parameters. Adv. Space Res. 42, 599–609.

Brooke, J. S. A., Bernath, P. F., Western, C. M., Sneden, C., Afşar, M., Li, G., Gordon, I. E., 2016. Line strengths of rovibrational and rotational transitions in the $X^2\Pi$ ground state of OH. J. Quant. Spect. Rad. Transfer 168, 142–157.

Bruggeman, P., Verreycken, T., Á González, M., Walsh, J. L., Kong, M. G., Leys, C., Schram, D. C., 2010. Optical emission spectroscopy as a diagnostic for plasmas in liquids: opportunities and pitfalls. J. Phys. D: Appl. Phys 43, 214005.

Brunger, M. J., 2017. Electron scattering and transport in biofuels, biomolecules and biomass fragments. Int. Rev. Phys. Chem. 36, 333–376.

Brunger, M. J., Buckman, S. J., 2002. Electron–molecule scattering cross sections. I. Experimental techniques and data for diatomic molecules. Phys. Rep. 357, 215–458.

Campbell, L., Brunger, M. J., 2013. Modelling of plasma processes in cometary and planetary atmospheres. Plasma Sources Sci. Technol. 22, 013002.

Campbell, L., Brunger, M. J., 2016. Electron collisions in atmospheres. Int. Rev. Phys. Chem. 35, 297–351.

Campbell, L., Cartwright, D. C., Brunger, M. J., Teubner, P. J. O., 2006. Role of electronic excited N_2 in vibrational excitation of the N_2 ground state at high latitudes. J. Geophys. Res. 111, A09317.

Charters, P. E., Macdonald, R. G., Polanyi, J. C., 1971. Formation of vibrationally excited OH by the reaction H + O_3. Appl. Opt. 10, 1747–1754.

Chen, X., Morgan, L. A., 1997. Low-energy electron scattering from the X $^2\Pi$ state of the OH molecule. J. Phys. B: At. Mol. Opt. Phys. 30, 3709–3717.

Drawin, H. W., 1968. Collision and transport cross-sections. In: Lochte-Holtgreven, W. (Ed.), Plasma Diagnostics. North-Holland Pub. Co., Amsterdam.

French, W. J. R., 2002. Hydroxyl airglow temperatures above Davis Station, Antarctica. Ph.D. thesis, University of Tasmania and the Australian Antarctic Division.

French, W. J. R., Klekociuk, A. R., 2011. Long-term trends in Antarctic winter hydroxyl temperatures. J. Geophys. Res. 116, D00P09.

Greer, R. G. H., Murtagh, D. P., McDade, I. C., Dickinson, P. H. G., Thomas, L., Jenkins, D. B., Stegman, J., Llewellyn, E. J., Witt, G., Mackinnon, D. J., Williams, E. R., 1986. ETON 1: a data base pertinent to the study of energy transfer in the oxygen nightglow. Planet. Space Sci. 34, 771–788.

Greet, P. A., French, W. J. R., Burns, G. B., Williams, P. F. B., Lowe, R. P., Finlayson, K., 1998. OH(6–2) spectra and rotational temperature measurements at Davis, Antarctica. Ann. Geophys. 16, 77–89.

Grygalashvyly, M., 2015. Several notes on the OH* layer. Ann. Geophys. 33, 923–930.

Harang, O., Pettersen, H., 1967. Variation in width of the H_α line in aurora. Planet. Space Sci. 15, 1599–1603.

Harrison, A. W., 1970. Behavior of hydroxyl emission during aurora. J. Geophys. Res. Space Phys. 75, 1330–1333.

Hedin, A. E., 1991. Extension of the MSIS thermosphere model into the middle and lower atmosphere. J. Geophys. Res. 96, 1159–1172.

Herzberg, G., 1989. Molecular Spectra and Molecular Structure I. Spectra of Diatomic Molecules, 2nd Edition. Kreiger, Malabar, Florida.

Makabe, T., Petrovic, Z. L., 2014. Plasma Electronics: Applications in Microelectronic Device Fabrication, 2nd Edition. CRC Press, Boca Raton.

McDade, I. C., Llewellyn, E. J., Murtagh, D. P., Greer, R. G. H., 1987. ETON 5: simultaneous rocket measurements of the OH Meinel $\Delta\nu = 2$ sequence and (8,3) band emission profiles in the nightglow. Planet. Space Sci. 35, 1137–1147.

McEwen, D. J., Venkatarangan, P., 1978. Electron flux and auroral intensity measurements in situ. Geophys. Res. Lett. 5, 1051–1054.

Meinel, A. B., 1950a. *OH* emission bands in the spectrum of the night sky. I. Ap. J. 111, 555–564.

Meinel, A. B., 1950b. *OH* emission bands in the spectrum of the night sky. II. Ap. J. 112, 120–130.

Migliorini, A., Gérard, J. C., Soret, L., Piccioni, G., Capaccioni, F., Filacchione, G., Snels, M., Tosi, F., 2015. Terrestrial OH nightglow measurements during the Rosetta flyby. Geophys. Res. Lett. 42, 5670–5677.

Miyoshi, Y., Oyama, S., Saito, S., Kurita, S., Fujiwara, H., Kataoka, R., Ebihara, Y., Kletzing, C., Reeves, G., Santolik, O., Clilverd, M., Rodger, C. J., Turunen, E., Tsuchiya, F., 2015. Energetic electron percipitation associated with pulsating aurora: EISCAT and Van Allen Probe observations. J. Geophys. Research: Space Phys. 120, 2754–2766.

Nicolet, M., 1970. Ozone and hydrogen reactions. Ann. Géophys. 26, 531–546.

Noble, C. J., Higgins, K., G. Wöste, Duddy, P., Burke, P. G., Teubner, P. J. O., Middleton, A. G., Brunger, M. J., 1996. Phys. Rev. Lett. 76, 3534–3537.

Osterbrock, D. E., Fulbright, J. P., 1998. Faint OH ($\nu' = 10$), ^{17}OH, and ^{18}OH emission lines in the spectrum of the night airglow. Publ. Astron. Soc. Pac. 110, 1499–1510.

Phillips, F., Burns, G. B., French, W. J. R., Williams, P. F. B., Klekociuk, A. R., Lowe, R. P., 2004. Determining rotational temperatures from the OH(8-3) band, and a comparison with OH(6-2) rotational temperatures at Davis, Antarctica. Ann. Geophys. 22, 1549–1561.

Riahi, R., Teulet, Ph., Ben Lakhdar, Z., Gleizes, A., 2006. Cross-section and rate coefficient calculation for electron impact excitation, ionisation and dissociation of H_2 and OH molecules. Eur. Phys. J. D 40, 223–230.

Romick, G. J., 1973. The hydroxyl emissions in relation to the dynamical processes of the atmosphere. Tech. Rep. NASA-CR-130237, NASA.

Sigernes, F., Shumilov, N., Deehr, C. S., Nielsen, K. P., Svenøe, T., Havnes, O., 2003. Hydroxyl rotational temperature record from the auroral station in Adventdalen, Svalbard (78°N, 15°E). J. Geophys. Res. 108, 1342.

Suzuki, H., Tsutsumi, M., Nakamura, T., Taguchi, M., 2010. The increase in OH rotational temperature during an active aurora event. Ann. Geophys. 28, 705–710.

Takahashi, H., Batista, P. P., 1981. Simultaneous measurements of OH(9,4), (8,3), (7,2), (6,2) and (5,1) bands in the airglow. J. Geophys. Res. 86, 5632–5642.

Teulet, P., Sarrette, J. P., Gomes, A. M., 1999. Calculation of electron impact inelastic cross sections and rate coefficients for diatomic molecules. Application to air molecules. J. Quant. Spect. Rad. Transfer 62, 549–569.

Turnbull, D. N., Lowe, R. P., 1989. New hydroxyl transition probabilities and their importance in airglow studies. Planet. Space Sci. 37, 723–738.

Vallance Jones, A., 1974. Aurora. D. Reidel Publishing Company, Dordrecht, Holland.

Xu, J., Gao, H., Smith, A. K., Zhu, Y., 2012. Using TIMED/SABER nightglow observations to investigate hydroxyl emission mechanisms in the mesopause region. J. Geophys. Res. 117, D02301.

Zammit, M. C., Savage, J. S., Fursa, D. V., Bray, I., 2017. Electron-impact excitation of molecular hydrogen. Phys. Rev. A 95, 022708.

- Electron-impact vibrational excitation cross sections are calculated for OH
- Application to mesospheric OH does not explain observations
- Discrepancies with previous calculations show need for measurements